J Appl Electrochem (2014) 44:159–168
DOI 10.1007/s10800-013-0619-1

RESEARCH ARTICLE

Electrochemical performance of nanoporous Si as anode for lithium ion batteries in alkyl carbonate and ionic liquid-based electrolytes

S. Ivanov · C. A. Vlaic · S. Du · D. Wang · P. Schaaf · A. Bund

Received: 7 June 2013 / Accepted: 18 August 2013 / Published online: 30 August 2013

Abstract Nanoporous Si was obtained by means of metal-assisted chemical etching. Li ion insertion–extraction was tested by voltammetric and galvanostatic electrochemical cycling in conventional 1 M $LiPF_6$ ethylene carbonate/dimethyl carbonate EC/DMC and in 1 M LiTFSI 1-butyl-1-methyl-pyrrolidinium bis (trifluoromethyl) sulfonylimide [BMP] [TFSI] electrolytes. The nanoporous Si demonstrated high reversibility when cycled in 1 M $LiPF_6$ EC/DMC electrolyte and showed superior activity compared to the non-structured sample. In contrast to the organic carbonate electrolyte, the material cycling in ionic liquid media showed reduced capacity and reversibility of the Li ion exchange. The latter results were discussed in terms of the high viscosity of the ionic liquid and ineffective cathodic passivation of the Si substrate in the ionic liquid-based electrolyte. Scanning electron microscopy imaging showed minor morphological changes due to the large volume change during Li insertion. No signs of crack formation and propagation were detected during the time span of the measurement.

Keywords Nanoporous Si · Lithium ion battery · Metal-assisted chemical etching · Li–Si alloying · Ionic liquid

S. Ivanov (✉) · C. A. Vlaic · A. Bund
Department of Electrochemistry and Electroplating, Ilmenau University of Technology, Gustav-Kirchhoff-Str. 6, 98693 Ilmenau, Germany
e-mail: svetlozar-dimitrov.ivanov@tu-ilmenau.de

S. Du · D. Wang · P. Schaaf
Department of Materials for Electronics, Ilmenau University of Technology, Gustav-Kirchhoff-Str. 5, 98693 Ilmenau, Germany

1 Introduction

The development of new active materials for Li ion batteries with improved performance is crucial due to the considerable demand for high power and energy applications. Other key aspects related to the increasing interest in high-performance battery materials are the environmental issues arising as a consequence of electrical energy production and significance of renewable energy storage [1].

The main challenge in the progress of advanced electrode materials is to design structures displaying both high lithium-storage capacity and long-term cycling stability. The currently used commercial graphite anode has good cycling performance, but a comparatively low specific capacity of 372 mAh g^{-1}. Li alloys [2–9], extensively researched initially at elevated temperatures [2, 4, 5], have been suggested as an alternative to Li metal and graphite anodes in Li ion batteries operating with organic electrolytes [1, 3, 4, 7–9]. Along different Li alloys, Li–Si attracts great interest because of its very high specific capacity for electrochemical formation. The theoretical capacity of Si is about 4200 mAh g^{-1}, one of the highest values among the anode materials for lithium ion batteries [6, 8, 9]. Nevertheless, the main disadvantage of Si is the large volume expansion accompanying the process of Li^+ insertion into the structure, inducing a rapid capacity fade and degradation of the electrode [8].

Various approaches have been undertaken to improve the cycling stability of Si-based electrodes, including decreasing the active layer thickness [10, 11], limitation of state of charge of Si anodes by means of capacity or voltage control [12–14], improving the adhesion and increasing the conductivity of the layer [15, 16]. It was shown that amorphous Si layers can accommodate Li ions rapidly and reversibly with lesser capacity loss in

comparison with crystalline ones [8, 17, 19]. Electrochemical Li exchange in Si was further investigated for different types of Si composites and thin films containing carbon, metals, electrochemically inactive components or alloys in their structures [8]. Most of these approaches resulted in an improved cyclability of the electrodes.

In addition to these methods, a considerable number of studies dealing with Si-based anodes are focused on nanostructured Si [21–33]. Nanoscale dimensions of Si anodes tolerate quick relaxation of the mechanical stress induced by the lithiation process, and consequently, nanoparticles resist better to fracture than bulk material [23]. Furthermore, due to the increased surface-to-volume ratio and shorter Li ion diffusion length, the rate capability and specific capacity of the material are considerably enhanced. Additionally, the design of nanoscaled materials may reduce the electrode polarization during Li ion insertion [24]. For example, Si nanowires and nanotubes have shown stable multiple cycling and reversible capacities around 3400 mAh g^{-1} [26]. Several procedures were used to produce or to nanostructure silicon nanoparticles such as: ball-milling [34], magnesiothermic reduction [35], wet chemical etching [36], electrochemical etching [23, 28], or metal-assisted chemical etching [27, 37]. Nanoparticulate nanoporous silicon combined with conductive additive and binders were investigated as anodes for LIBs, showing high energy storage capacity of 2050 mA h g^{-1} at a rate of 0.2 C and remarkable coulombic efficiency of 94.4 % [37].

Apart from the Si composite anodes consisting of integrated Si powder, the particular interest in surface nanostructured planar Si is motivated by the potential to implement this anode material in microbatteries [9, 38, 39]. Surface nanostructured Si provides high specific surface area, which enables fast transport of Li ions. In addition, the volume expansion can be well accommodated by the nanostructured Si during lithiation. It was reported that multiple reversible Li insertion–extraction in nanostructured crystalline Si can be successfully performed without disintegration of the substrate. Nevertheless, the process of Li exchange is restricted by diffusion through the Zintl phase compound (ZPC) layer [9]. It was concluded that without surface structuring, the material is hardly applicable due to low charge/discharge rate capability. For achieving a good performance for applications in microbatteries, a large contact area of Si/electrolyte interface accomplished by surface structuring is necessary.

Along with several other techniques for Si nanostructuring such as anodic etching, chemical stain etching, chemical vapor etching and laser-induced etching [29] metal-assisted chemical etching (MaCE) gained recently an increased attention [29–33]. Since the pioneering work of Dimova-Malinovska [30], where the method of Si stain etching was further developed by introducing a thin Al film on the Si surface acting as a catalyst, the influence of different metals (Ag, Au, Pt) on the etching process was extensively studied [33]. In MaCE, Si is previously modified usually by electroless or physical vapor deposition of a thin noble metal layer, followed by chemical etching in an aqueous solution consisting of HF and an oxidant (e.g., H_2O_2 or $AgNO_3$) to form porous silicon or silicon nanowires. The chemical reactions during the process of metal-assisted Si etching are generally considered to take place at the interface Si/noble metal. By using this approach, the considerable induction time, characteristic for normal stain etching, can be significantly reduced, and the etching rate is accelerated by the catalytic effect of the noble metal. Depending on the exact specific conditions, MaCE can fast produce different types of nanoporous structured silicon with a broad variety of aspect ratios [29, 33]. MaCE has additional advantages related to the economical and energy aspects of the nanoporous Si fabrication. The technique is fast, characterized by low energy consumption and does not require expensive and complicated equipment [33].

Another key aspect of Li ion battery technology is the development of advanced and reliable electrolyte solutions for high power- and energy-storage systems. It was shown that the commonly used organic carbonate-based electrolytes can induce operational and safety issues, since they are flammable, and the onset of their electrochemical oxidation can be below 4 V versus Li/Li^+, depending on the substrate [40–43]. Additionally, the thermal instability of alkyl carbonate solvents was confirmed [44].

One useful alternative to the conventional electrolytes applied for Li ion batteries are ionic liquids (ILs) containing a Li salt [18–20, 45–53]. The increasing interest in this relatively new class of substances is motivated by the attractive combination of their physical properties. They exhibit very low vapor pressure; at the same time, they are non-flammable, and some of them have excellent electrochemical stability, displaying a considerably extended anodic potential limit, which can improve the operational and thermal stability of the battery.

Nevertheless, still open issues such as high viscosity, low conductivity and high costs make the application of ILs a remaining challenge [45]. Generally, considering the cathodic instability of organic electrolytes for Li ion batteries, ILs are not an exception. Similarly to the organic carbonate electrolytes, in a number of cases, ILs were combined with additives in order to achieve stable cathodic passivation and improvement of the cyclability [45–48]. The possibility to implement IL for application in 5 V Li ion batteries was investigated [19, 20]. The larger potential window of the ILs in comparison with carbonate-based electrolytes was demonstrated, and it was found that the active material performance regarding the mechanism,

kinetics and efficiency of their passivation in ionic liquid electrolytes is related to the particular characteristics of both IL and electrode material [45, 51].

Detailed studies on the electrochemistry of anode materials in ILs were completed for graphite [45–47], $Li_4Ti_5O_{12}$ (LTO) [19, 45, 50, 51], TiO_2[53] and metallic Li [45, 49]. Particularly, for Si-based anodes, there is limited number of investigations on their cyclability in ILs [18, 45, 48], and according to our knowledge, the electrochemical properties of nanostructured Si are still not approached in Li ion containing IL media.

In this work, we demonstrate the possibility to apply nanoporous silicon fabricated using MaCE for electrochemical cycling in Li ion containing electrolytes. The main focus of the study is the impact of thin layer surface nanostructuring on the electrochemical activity of Si electrode for Li ion exchange, considering the influence of electrolyte type. In current research, the fabricated nanoporous Si was tested in both 1 M $LiPF_6$ EC/DMC and IL electrolyte (1 M LiTFSI, 1-butyl-1-methyl-pyrrolidinium bis (trifluoromethyl) sulfonylimide [BMP][TFSI] for comparison. The type of IL was chosen on the basis of the well-known high electrochemical stability of [BMP][TFSI]. The electrochemical window of [BMP][TFSI] ranges from about 0 to 5 V exhibiting an excellent performance of its both anion and cation components [40, 45].

2 Experimental

2.1 Chemicals and reagents

The chemicals for metal-assisted chemical etching (HF, H_2O_2, KI, I_2) were purchased from Merck. EC, DMC, $LiPF_6$ and LiTFSI were obtained from Alfa Aesar. [BMP][TFSI] was purchased from IoLiTec (Heilbronn, Germany). All reagents and [BMP][TFSI] used in the electrochemical experiments were dried under argon atmosphere until a value of 15 ppm H_2O was reached. The water content in the electrolyte solutions was monitored by Carl—Fisher titration by using an 831 KF Coulometer (Metrohm).

2.2 Metal-assisted chemical etching

(111)-oriented p-Si wafers (Boron doped, resistivity of 0.001–0.0025 Ω cm, CEMAT S.A.) were used for fabrication of thin layers of nanoporous Si. The wafers were cut into squares of 1.5×1.5 cm^2, and the samples were cleaned with acetone and isopropanol. A 20-nm-thick Au film was deposited onto the Si samples via electron beam evaporation. Then, the samples were immersed for 5 min in an aqueous solution consisting of 5 M HF and 0.3 M H_2O_2 for MaCE. About 400-nm-thick layers of nanoporous Si were formed with pore/ligament size around 10 nm. Then, the samples were immersed in an aqueous solution consisting of 0.6 M KI and 0.09 M I_2, in order to remove the remaining Au. Finally, the samples were rinsed with deionized water for about 5 min and then dried with N_2.

2.3 Electrochemical measurements and scanning electron microscopy (SEM)

Both nanoporous and non-structured samples (same Si wafer without MaCE) were electrochemically characterized using a potentiostat/galvanostat Biologic VMP3 in a three electrode configuration. The samples were cycled within a potential range 2–0.02 V versus Li metal reference electrode. The galvanostatic measurements were carried out at different constant currents between 1.2 and 0.05 V. A home-made PTFE electrochemical cell equipped with Li metal counter and reference electrodes was used for electrochemical tests. The geometric area of the working electrode was 0.27 cm^{-2}. The cell assembly and electrochemical measurements were performed in a glove-box (M-Braun) maintaining H_2O and O_2 levels below 0.1 ppm. The samples were investigated using an ultrahigh resolution scanning electron microscope (FE-SEM, Hitachi S-4800). Thin amorphous Si sample was prepared by magnetron sputtering on Ti foil substrate.

3 Results and discussion

The electrochemical activity of both nanoporous and non-structured Si samples was initially investigated by means of cyclic voltammetry in 1 M $LiPF_6$ EC/DMC (1/1) v/v electrolyte (Fig. 1).

The voltammetric curves display the characteristic current peaks for Si–Li alloying/dealloying in the potential range 1–0 V. A considerable difference between the first and the following voltammetric cycles was observed. The presence of an irreversible cathodic process during the first cycle with onset at about 1.7 V can be attributed to the formation of a passive solid-electrolyte interfacial (SEI) layer at the sample surface, typical for low potential anode materials (e.g., graphite, Si and metallic Li) cathodically polarized in organic carbonate electrolytes [43, 44]. It is well known that the passivation of conventional organic carbonate-based electrolytes starts at about 0.8 V versus Li^+ Ref. [56] However, this potential can vary depending on the type of the substrate. Aurbach et al. [57] in their review article on electrolytes for Li ion batteries emphasize that all negative electrodes that function at potentials below 1.5 V (Li/Li^+) should react with electrolyte and become

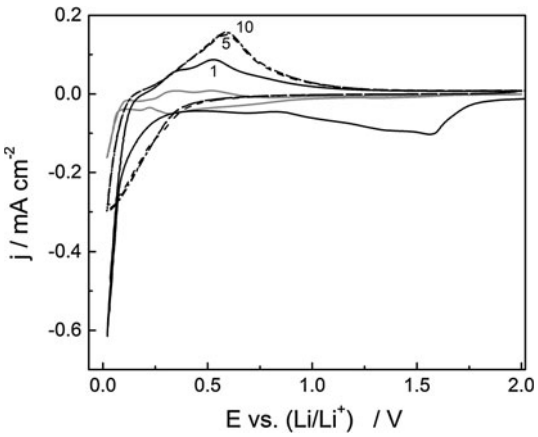

Fig. 1 Consecutive voltammetric cycles of nanoporous Si—first cycle (*black*), fifth (*dash*) and tenth (*dash dot*) and non-structured Si electrode first cycle (*gray*) measured in 1 M $LiPF_6$ EC/DMC (1:1)v/v. Scan rate 0.5 mV/s

covered by passive surface films comprising insoluble products. Nevertheless, in the particular case of nanostructured silicon, due to the high surface area, the formation of SEI layer can be more pronounced, expressed by enhanced currents. Furthermore, the extension of the onset of SEI formation to more positive potential values could be due to catalytic activity of the substrate, which probably contains traces of Au resting from MaCE procedure. Similarly to the results presented in this study, it was reported that at different types of nanostructured Si electrodes, the cathodic surface passivation starts in the potential range between 1.4 and 1.6 V [28, 34, 35].

In addition, a gradual increase in the current density during the first several potential sweeps followed by saturation of the peak current values was observed. The enhancement in the electroactivity during cyclic voltammetry of the Si samples can be associated with the initial phase transition of crystalline to amorphous Si, developing of the phase transition front and increase in the Si amount taking part in the alloying–dealloying process. The attainment of steady state cycling after the fifth voltammetric cycle suggests contribution of constant quantity of Si in the process of lithiation. Similar observation has been reported for sub-micro-sized pillar arrays fabricated on Si substrates studied in 1 M $LiClO_4$, EC/DEC electrolyte [9]. A noticeable difference can be seen in voltammetric activity between nanoporous and the non-structured sample. The nanoporous Si showed higher peak currents than the flat Si sample, making evident the superior cycling behavior of the nanostructured material. This result is a consequence of larger active surface area of the nanoporous Si and more efficient transport of the Li ions in the porous structure. The cause of such a low electroactivity of the planar crystalline Si can be attributed to the very slow solid-state diffusion of lithium ions in the crystal lattice. Practically, the lithium alloying occurs in a very thin external layer of the Si wafer, while nearly entire material amount is not involved in the process of Li insertion [17].

Both types of samples were further tested in the IL electrolyte (1 M LiTFSI, [BMP][TFSI]), and the voltammetric curves are shown in Fig. 2. The first cathodic sweep showed irreversible reduction process similar to the passivation phenomena in case of EC/DMC-based electrolyte; however, in IL electrolyte, the process starts much later at potential about 1 V. In our previous study on the performance of TiO_2 self-organized nanotubes in ionic liquid electrolyte [53], we have investigated the potential window of pristine and Li ion containing [BMP][TFSI] on Ti electrode. We have shown that decomposition of pure [BMP][TFSI] starts at about 1 V. However, it was observed that after addition of LiTFSI, the metal electrode passivates very efficiently in the first cathodic sweep (between 0 and 1 V), and reversible Li deposition/dissolution take place very close to 0 V. This result stays in good agreement with the anodic stability of [BMP][TFSI] on platinum and glassy carbon substrates [49].

Based on the stability potential window of the IL electrolyte, we can assume that the cathodic peak at 0.6 V (Fig. 2) display SEI layer formation since it overlaps with the potential passivation range of Li[TFSI] [BMP]TFSI] electrolyte. Nevertheless, exact determination of the cathodic peak origin, correlating it with specific potential is rather challenging task due to the substrate influence, its specific surface chemistry and catalytic properties.

Generally, the current response is much lower in 1 M Li[TFSI] [BMP][TFSI] than in 1 M $LiPF_6$ EC/DMC. This can be explained by the different viscosity of both electrolytes. The viscosities of [BMP][TFSI] and EC/DMC are 0.060 and 0.001 Pa s, respectively [45, 46]. The high

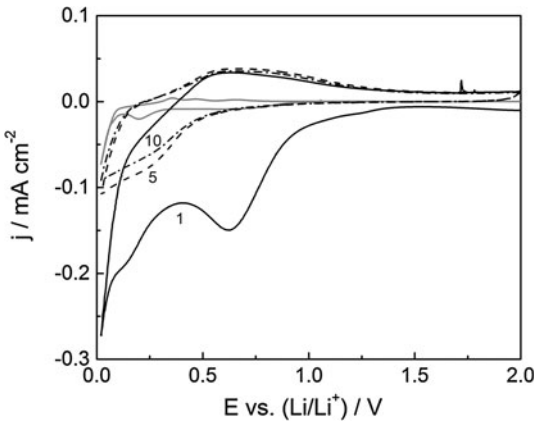

Fig. 2 Consecutive voltammetric cycles of nanoporous Si: first cycle (*solid*), fifth (*dashed*) and tenth (*dotted*) and non-structured Si electrode (*gray lines*) measured in 1 M Li[TFSI] [BMP][TFSI]. Scan rate 0.5 mV/s

viscosity of the IL induces slow ion mobility, limiting the amount of Li^+ available for alloying in the nanoporous Si layer. The hindered dynamic of Li ion exchange in the nanoporous Si structure is also indicated by the potential shift and increasing of the peak-to-peak potential difference of the voltammetric waves in case of nanoporous Si cycled in LiTFSI, [BMP] [TFSI]. Other possible reasons for the lower peak currents observed in LiTFSI, [BMP] [TFSI] could be the irreversible formation of products during potential cycling and co-intercalation of compounds originating from the IL. The latter phenomena were studied in detail by means of in situ Raman spectroscopy performed in the course graphite cycling in LiTFSI, [BMP] [TFSI] and 1-methyl-propylpiperidinium bis(trifluoromethyl sulfonyl)imide [MPPp][TFSI] [52]. It was confirmed that [BMP][TFSI] can be electrochemically reduced during Li ion insertion, resulting in the formation of a number of different types of insoluble compounds [19, 52], which most likely increase the charge transfer resistance and limit the Li ion mobility in the porous nanostructure. One additional appropriate example related to this phenomenon is given by Sugimoto et al. [18], where the application of bis(fluorosulfonyl)imide (FSI) and bis(trifluoromethanesulfonyl)imide (TFSI) anions as an electrolyte component for Li ion batteries was studied. It was found that the FSI-based ionic liquids can effectively present a long-term reversible cycling of Si–Ni–C anode comparable to the performance observed in a conventional carbonate-based electrolyte. In contrast, ILs containing bis(trifluoromethanesulfonyl)imide (TFSI) anion showed no reversible capacity. The observed phenomena were ascribed to deposition of a blocking layer which increases the interfacial resistance of the Si–Ni–C anode.

The charge/discharge capacity and the coulomb efficiency of the process evaluated from the cyclic voltammetry are presented versus cycle number and summarized in Fig. 3a, b.

It can be seen that the variation of the discharge capacity of nanoporous samples in 1 M $LiPF_6$, EC:DMC electrolyte (about 5 μAh cm^{-2}) is two times lower than those for the non-structured sample. At the same time, the flat Si sample shows identical behavior in both Li ion containing electrolytes, displaying lower electroactivity than the nanoporous Si sample. This outcome suggests better electrochemical performance of the nanoporous structures during the initial stages of lithiation/delithiation. It can be seen that the current efficiency at the beginning of the cycling (first 2–3 cycles) is generally very low for all samples (Fig. 3b). It is evident that the current efficiency of nanoporous Si sample in EC/DMC electrolyte increases more rapidly in comparison with the sample cycled in IL, reaching a value of about 90 % at third cycle. The latter observation suggests that at that early period of cycling, the formation of SEI layer is to a high extent completed, and the material is stable during the subsequent cycles. Contrary to EC/DMC electrolyte, the cycling in ionic liquid showed much less efficiency, slowly approaching 86 %. This result indicates that the cathodic passivation process is not finalized in the timescale of the voltammetric experiment, very probably due to the slow penetration of the electrolyte into the porous Si structure. Another possible reason for the reduced efficiency of the nanoporous sample in IL electrolyte could be mechanical instability of the interface (cracking of the surface during lithiation) induced by the internal tension during Li ion insertion. Nevertheless, cracking of the material was not observed by SEM imaging of cycled nanoporous Si samples. Hence, the lower current efficiency in case of nanoporous Si cycled in ionic liquid is most likely related to retarded penetration of the viscous electrolyte inside the inner nanopores, which does not allow completion of the surface passivation.

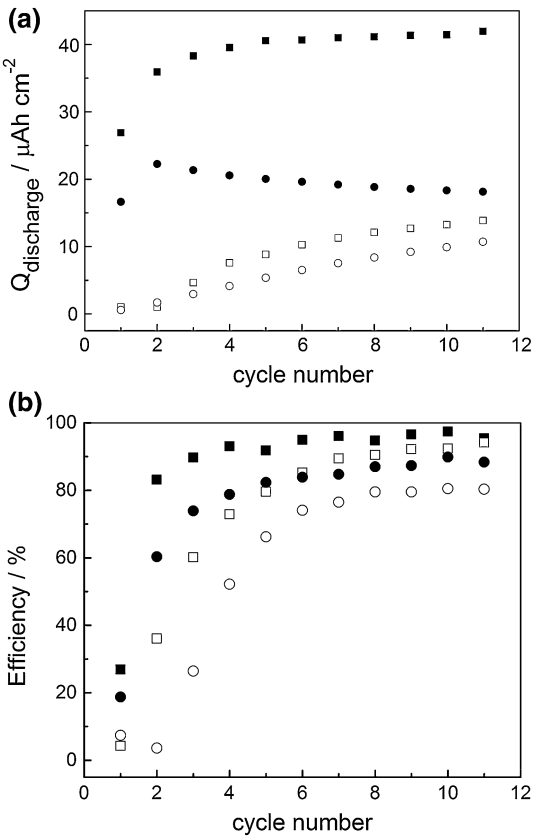

Fig. 3 **a** Discharge capacity dependence on cycle number calculated from voltammetric curves measured in 1 M $LiPF_6$ EC/DMC for nanoporous (*filled square*) and non-structured Si electrode (*open square*) and in 1 M Li[TFSI] [BMP][TFSI] for nanoporous (*filled circle*) and non-structured Si electrode (*open circle*) Fig. 3b. Current efficiency of nanoporous Si calculated from cyclic voltammetry in 1 M $LiPF_6$ EC/DMC (*filled square*) and 1 M Li[TFSI] [BMP TFSI] (*filled circle*) and for non-structured Si electrode in 1 M $LiPF_6$ EC/DMC (*open square*) and 1 M Li[TFSI] [BMP TFSI] (*open circle*)

A further step in our study was to quantify the amount of energy stored in the nanoporous Si layer. It is well known that the evaluation of the specific capacity obtained during potential cycling of single Si crystals (i.e., Si wafer) is a challenging task due to continuous penetration of Li ions into the bulk Si and the parallel process of possible material cracking leading to morphological transformations of the electrode [8, 17]. The above discussed phenomena induce a continuous dynamic change of the Si amount undergoing electrochemical lithiation. Thus, the contribution of the Si (non-structured) substrate is difficult to estimate. Nevertheless, it was found that the Li ion storage in planar single Si crystal in the course of galvanostatic cycling is about 0.1 Ah g^{-1}. Considering the mass of the entire Si crystal, this value is equal to only 2 % of the theoretical Si capacity. The reason for this result was attributed to the very slow solid-state diffusion of Li ions in the crystal lattice [17]. Furthermore, study on electrochemical performance of macroporous Si performed by Thamkur et al. [54] suggests that the bulk Si underlying substrate is not involved in the Li ion exchange, and hence, the porous Si upper layer plays a protective effect for the electrode stability. Based on the discussion above and the significant difference between the obtained areal capacities of nanoporous and non-structured Si, a negligible impact of the Si substrate in the case of nanoporous Si can be assumed. Additionally, signs of cracks and structural disintegration of the electrode were not observed in the time span of the experiment.

In order to determine the specific capacities of the nanoporous Si layer, a porosity value of 74 % related to the obtained pore diameter was considered [29, 55]. Porosity yielding about 70–75 % was confirmed gravimetrically.

Nanoporous and the non-structured silicon were galvanostatically cycled in EC/DMC (Fig. 4a) and IL (Fig. 4b)-based electrolytes. The electrodes were initially activated by performing a galvanostatic cycle at $i = 100$ μA cm^{-2} and further cycled at $i = 0.25$ and 0.4 mA cm^{-2}.

The data for discharge capacities are summarized in Fig. 5. The values obtained for the first discharge cycles

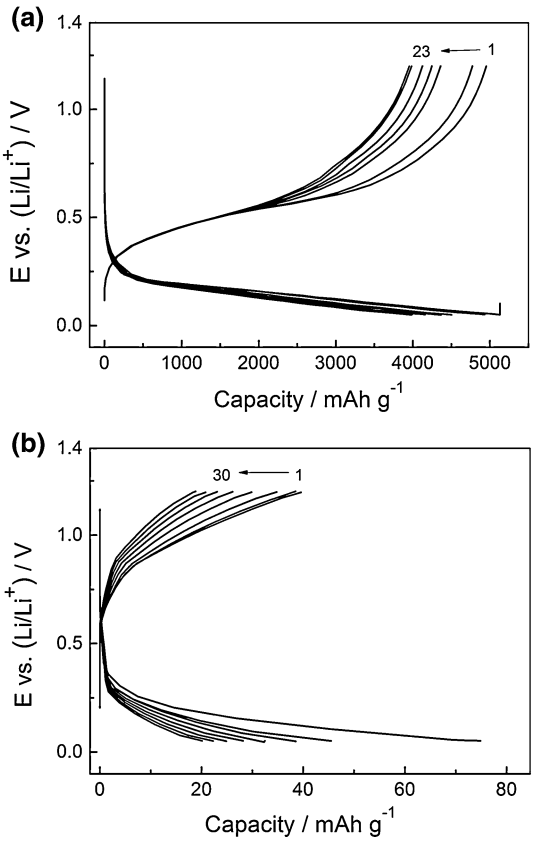

Fig. 4 **a** Galvanostatic charge/discharge curves for the first and up to the twenty-third cycle at 0.4 mA cm^{-2} in 1 M $LiPF_6$, EC/DMC Fig. 4b. Galvanostatic charge/discharge curves for the first and up to the eighth cycle at 0.125 $mAcm^{-2}$ in 1 M Li[TFSI] [BMP TFSI]

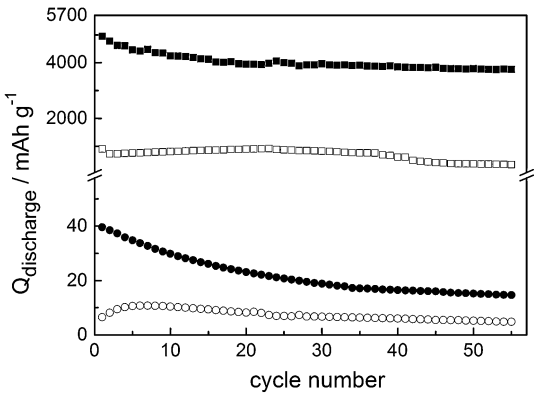

Fig. 5 Discharge capacity calculated from galvanostatic curves as a function of cycle number for nanoporous Si in 1 M $LiPF_6$ EC/DMC (*filled square*), 1 M Li[TFSI] [BMP TFSI] (*filled circle*) and for non-structured Si in 1 M $LiPF_6$ EC/DMC (*open square*), 1 M Li[TFSI] [BMP TFSI] (*open circle*) correspondingly

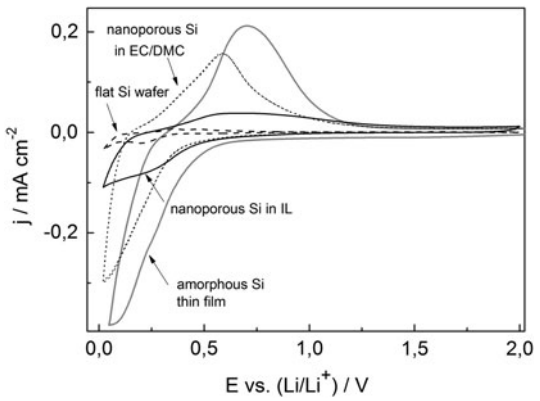

Fig. 6 Cyclic voltammetry of nanoporous Si (*black*), amorphous Si thin film (*gray*), non-structured Si electrode (*dash*) measured in 1 M LiTFSI [BMP TFSI] and nanoporous Si measured in 1 M $LiPF_6$ EC/DMC (*dot*). Scan rate 0.5 mV/s

(≈4700 mAh/g) suggest that there is also a small contribution of about 10 % given by the underlying silicon substrate. The galvanostatic cycling carried out in both carbonate and IL-based electrolytes displayed reversible lithiation with coulombic efficiency in the range of 93–99 %. Similar to the data obtained by cyclic voltammetry, the results from nanoporous Si galvanostatic cycling in IL showed considerably lower capacity in comparison with the sample cycled in EC/DMC. The nanoporous Si in EC/DMC-based electrolyte showed 20 % capacity fade during 30 galvanostatic cycles, reaching stable values of 3900 $mAhg^{-1}$ (Fig. 5). The results for discharge capacity and current efficiency obtained in the current study are in a good agreement with the data reported in literature [9, 25, 28]. Highly ordered nanoporous Si fabricated combining direct nanoimprint with subsequent galvanostatic etching showed a columbic efficiency of about 70 % in the first cycle; however, the anode showed reversible galvanostatic cycling without disintegration only when Li insertion was limited to 1400 Ah g^{-1} [28]. 2500 mAh g^{-1} reversible capacities with excellent cycling stability (≈90 % capacity retention after 100 cycles) have been obtained in the case of a nanoporous silicon electrode fabricated by in situ thermal generation with triethanolamine as sacrificing template [25].

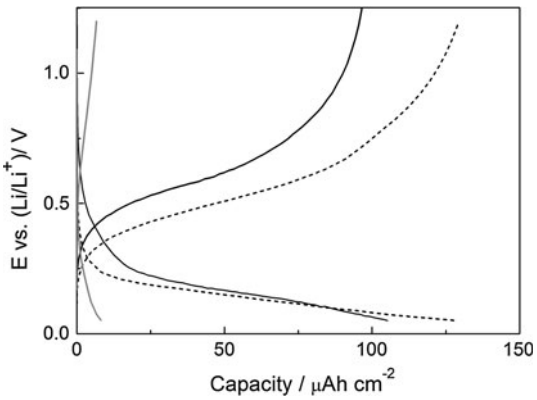

Fig. 7 Galvanostatic charge/discharge curves for amorphous Si thin film measured in 1 M $LiPF_6$ EC/DMC (*black*), nanoporous Si measured in 1 M $LiPF_6$ EC/DMC (*dash*) and nanoporous Si measured in 1 M Li[TFSI] [BMP TFSI] (*gray*)

In order to prove the cyclability of Si in 1 M LiTFSI, [BMP][TFSI] and study in more detail the suppressed lithium exchange in the case of nanoporous Si in ionic liquid electrolyte, an additional experiment of electrochemical lithiation of 400-nm-thick amorphous Si film sputtered by PVD on metallic substrate was carried out in IL electrolyte. The results from voltammetric (Fig. 6) and galvanostatic (Fig. 7) cycling showed reversible Si lithiation and increased current response of amorphous Si layer in comparison with nanoporous and non-structured Si samples.

Compared to nanoporous Si in 1 M LiPF6, EC:DMC, the amorphous thin Si layer displayed comparable areal capacity. Furthermore, specific capacity close to the theoretical value was evaluated from the galvanostatic cycling of the amorphous Si layer. The above discussed results

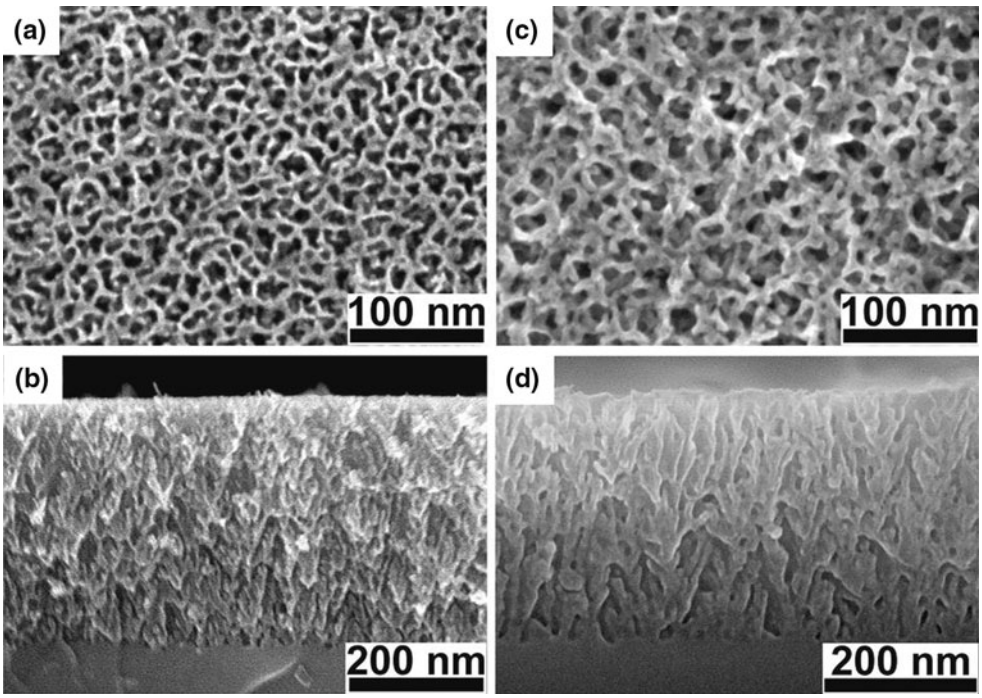

Fig. 8 SEM imaging of nanoporous Si before (**a**, **b**) and after (**c**, **d**) 10 voltammetric cycles performed in 1 M LiTFSI [BMP TFSI]

suggest that the specific combination of the ionic liquid components (BMP^+ and $TFSI^-$) is not the reason for hindered lithium ion exchange in the case of nanoporous Si, since amorphous Si displayed well-pronounced electrochemical behavior in 1 M LiTFSI, [BMP][TFSI]. Therefore, a probable reason for this phenomenon is the joint contribution of at least three factors influencing the Li ion dynamics in the porous Si structure: (1) high viscosity of the ionic liquid electrolyte, (2) the nanopore dimensions and (3) the crystalline nature of the nanoporous Si. A promising approach for preserving the high activity of the nanoporous Si could be the addition of components for lowering the viscosity, the design of Si structures with larger pore diameter and nanostructuring of amorphous Si.

Surface morphology of nanoporous Si before and after electrochemical cycling was investigated by SEM. Figure 8 shows the SEM images of the surface morphology of the nanoporous Si samples before electrochemical testing and after ten voltammetric cycles.

An increase in the ligament/pore size from about 10 to approximately 25 nm can be observed after the electrochemical cycling. This is probably due to a phase transformation from single crystalline to amorphous by the cycling. However, further SEM investigations show that in the case of nanostructured Si, there is no formation of ligaments micro-cracks neither of macro-cracks. In contrast, a considerable crack density was found for the non-structured electrodes after cycling. Therefore, the strain relaxation is much easier in the nanoporous structure which displays better cycling stability.

4 Conclusions

Nanoporous Si was obtained by MaCE of planar Si wafers. The method allows fast fabrication of thin Si nanoporous layers with adjustable thickness and porosity. Li ion insertion/extraction was tested by means of voltammetric and galvanostatic electrochemical cycling in conventional 1 M $LiPF_6$ EC/DMC and in 1 M Li[TFSI],[BMP][TFSI] electrolytes. Si nanoporous samples display high reversibility of the cycling in 1 M $LiPF_6$ EC/DMC electrolyte and have superior activity compared to the flat non-structured sample. The estimation of the charge/discharge capacity of the nanoporous layer suggests limited contribution of the underlying Si substrate which in turn is beneficial for the long-term stability of the electrode. The nanoporous Si measured in EC/DMC-based electrolyte displayed 20 % capacity fade during 30 galvanostatic cycles, reaching stable capacity values of 3900 $mAhg^{-1}$. The experiments performed in ionic liquid showed lower Si capacity and inferior reversibility of the cycling. The possible reason for the lower capacity in 1 M LiTFSI, [BMP][TFSI] could be summarized as interplay between the high viscosity of the ionic liquid, the narrow geometry of the nanostructured Si layer and the crystalline nature of nanoporous Si. The joint contribution of these three factors hinders the transport of the ions in the nanoporous structure. The surface morphology before and after the lithiation process of was characterized by SEM imaging. The micrographs showed morphological changes discussed in terms of structural volume change during Li insertion. No signs of crack formation and propagation were detected in the time span of the experiments.

Acknowledgments Financial support by the Grant (NanoBatt TNA VII-1/2012) from the state of Thuringia (TMWAT by LEG Thüringen), co-financed by the European Funds for Regional Development (EFRD) and the DFG funded program WeNDeLIB (project 6: *"Linking of model and commercial active materials for lithium ion batteries by in situ determination of thermodynamic and kinetic data"*) is gratefully acknowledged. The authors are thankful to B. Hartmann, I. Marquardt, J. Döll and R. Grieseler from Ilmenau University of Technology for their help with sample preparation.

References

1. Scrosati B, Hassoun J, Sun Y-K (2011) Lithium-ion batteries. A look into the future. Energy Environ Sci 4:3287–3295. doi:10.1039/C1EE01388B
2. Wen CJ, Huggins RA (1981) Chemical diffusion in intermediate phases in the lithium-silicon system. J Solid State Chem 37:271–278. doi:10.1016/0022-4596(81)90487-4
3. Yang J, Winter M, Besenhard JO (1996) Small particle size multiphase Li-alloy anodes for lithium-ion batteries. Solid State Ionics 90:281–287. doi:10.1016/S0167-2738(96)00389-X
4. Winter M, Besenhard JO (1999) Electrochemical lithiation of tin and tin-based intermetallics and composites. Electrochim Acta 45:31–50. doi:10.1016/S0013-4686(99)00191-7
5. Huggins RA (1999) Lithium alloy negative electrodes. J Power Sources 81–82:13–19. doi:10.1016/S0378-7753(99)00124-X
6. Bourderau S, Brouse T, Schleich DM (1999) Amorphous silicon as a possible anode material for Li-ion batteries. J Power Sources 81–82:233–236. doi:10.1016/S0378-7753(99)00194-9
7. Weydanz WJ, Wohlfahrt-Mehrens M, Huggins RA (1999) A room temperature study of the binary lithium–silicon and the ternary lithium–chromium–silicon system for use in rechargeable lithium batteries. J Power Sources 81–82:237–242. doi:10.1016/S0378-7753(99)00139-1
8. Kasavajjula U, Wang C, Appleby AJ (2007) Nano- and bulk-silicon-based insertion anodes for lithium-ion secondary cells. J Power Sources 163:1003–1039. doi:10.1016/j.jpowsour.2006.09.084
9. Green M, Fielder E, Scrosati B, Wachtler M, Moreno JS (2003) Structured silicon anodes for lithium battery applications. Electrochem Solid State Lett 6:A75–A79. doi:10.1149/1.1563094
10. Graetz J, Ahn CC, Yazami R, Fultz B (2003) Highly reversible lithium storage in nanostructured silicon. Electrochem Solid State Lett 6:A194–A197. doi:10.1149/1.1596917
11. Hatchard TD, Dahn JR (2004) *In Situ* XRD and electrochemical study of the reaction of lithium with amorphous silicon. J Electrochem Soc 151:A838–A842. doi:10.1149/1.1739217
12. Jung H, Park M, Yoon Y, Kim G, Joo S (2003) Amorphous silicon anode for lithium-ion rechargeable batteries. J Power Sources 115:346–351. doi:10.1016/S0378-7753(02)00707-3

13. Jung H, Park M, Han SH, Lim H, Joo S (2003) Amorphous silicon thin-film negative electrode prepared by low pressure chemical vapor deposition for lithium-ion batteries. Solid State Commun 125:387–390. doi:10.1016/S0038-1098(02)00849-9
14. Obrovac M, Krause L (2007) Reversible cycling of crystalline silicon powder. J Electrochem Soc 154:A103–A108. doi:10.1149/1.2402112
15. Ohara S, Suzuki J, Sekine K, Takamura T (2004) A thin film silicon anode for Li-ion batteries having a very large specific capacity and long cycle life. J Power Sources 136:303–306. doi:10.1016/j.jpowsour.2004.03.014
16. Uehara M, Suzuki J, Tamura K, Sekine K, Takamura T (2005) Thick vacuum deposited silicon films suitable for the anode of Li-ion battery. J Power Sources 146:441–444. doi:10.1016/j.jpowsour.2005.03.097
17. Kulova TL, Skundin AM, Pleskov YV, Terukov EI, Konkov OI (2007) Lithium insertion into amorphous silicon thin-film electrodes. J Electroanal Chem 600:217–225. doi:10.1016/j.jelechem.2006.07.002
18. Sugimoto T, Atsumi Y, Kono M, Kikutac M, Ishiko E, Yamagata M, Ishikawa M (2010) Application of bis(fluorosulfonyl)imide-based ionic liquid electrolyte to silicon–nickel–carbon composite anode for lithium-ion batteries. J Power Sources 195:6153–6156. doi:10.1016/j.jpowsour.2010.01.011
19. Baranchugov V, Markevich E, Pollak E, Salitra G, Aurbach D (2007) Amorphous silicon thin films as a high capacity anodes for Li-ion batteries in ionic liquid electrolytes. Electrochem Commun 9:796–800. doi:10.1016/j.elecom.2006.11.014
20. Markevich E, Baranchugov V, Aurbach D (2006) On the possibility of using ionic liquids as electrolyte solutions for rechargeable 5 V Li ion batteries. Electrochem Commun 8:1331–1334. doi:10.1016/j.elecom.2006.06.002
21. Kim I, Blomgren GE, Kumta PN (2003) Nanostructured Si/TiB2 composite anodes for Li-ion batteries. Electrochem Solid State Lett 6:A157–A161. doi:10.1149/1.1584212
22. Zhang Y, Fu Z-W, Qin Q-Z (2004) Microstructure and Li alloy formation of nano-structured amorphous Si and Si/TiN composite thin film electrodes. Electrochem Commun 6:484–491. doi:10.1016/j.elecom.2004.03.012
23. Shin H-C, Corno J, Gole J, Liu M (2005) Porous silicon negative electrodes for rechargeable lithium batteries. J Power Sources 139:314–320. doi:10.1016/j.jpowsour.2004.06.073
24. Aifantis KE, Hackney SA, Dempsey JP (2007) Design criteria for nanostructured Li-ion batteries. J Power Sources 165:874–879. doi:10.1016/j.jpowsour.2006.10.070
25. Du C, Gao C, Yin G, Chen M, Wang L (2011) Facile fabrication of a nanoporous silicon electrode with superior stability for lithium ion batteries. Energy Environ Sci 4:1037–1042. doi:10.1039/C0EE00428F
26. Szczech JR, Jin S (2011) Nanostructured silicon for high capacity lithium battery anodes. Energy Environ Sci 4:56–72. doi:10.1039/C0EE00281J
27. Ge M, Rong J, Fang X, Zhou C (2012) Porous doped silicon nanowires for lithium ion battery anode with long cycle life. Nano Lett 12:2318–2323. doi:10.1021/nl300206e
28. Nishio K, Tagawa S, Fukushima T, Masuda H (2012) Highly ordered nanoporous Si for negative electrode of rechargeable lithium-ion battery. Electrochem Solid State Lett 15:A41–A44. doi:10.1149/2.002204esl
29. Korotcenkov G, Cho BK (2010) Silicon porosification: state of the art. Crit Rev Solid State Mater Sci 35:153–260. doi:10.1080/10408436.2010.495446
30. Dimova-Malinovska D, Sendova-Vassileva M, Tzenov N, Kamenova M (1997) Preparation of thin porous silicon layers by stain etching. Thin Solid Films 297:9–12. doi:10.1016/S0040-6090(96)09434-5
31. Peng K, Hu J, Yan Y, Wu Y, Fang H, Xu Y, Lee S, Zhu J (2006) Fabrication of single-crystalline silicon nanowires by scratching a silicon surface with catalytic metal particles. Adv Funct Mater 16:387–394. doi:10.1002/adfm.200500392
32. Chartier Bastide S, Lévy-Clément C (2008) Metal-assisted chemical etching of silicon in HF–H_2O_2. Electrochim Acta 53:5509–5516. doi:10.1016/j.electacta.2008.03.009
33. Huang Z, Geyer N, Werner P, de Boor J, Gösele U (2011) Metal-assisted chemical etching of silicon: a review. Adv Mater 23:285–308. doi:10.1002/adma.201001784
34. Lv R, Yang J, Gao P, Nuli Y, Wang J (2010) Electrochemical behavior of nanoporous/nanofibrous Si anode materials prepared by mechanochemical reduction. J Alloy Compd 490:84–87. doi:10.1016/j.jallcom.2009.10.023
35. Gao P, Jia H, Yang J, Nuli Y, Wang J, Chen J (2011) Three-dimensional porous silicon–MWNT heterostructure with superior lithium storage performance. Phys Chem Chem Phys 13:20108–20111. doi:10.1039/c1cp23062j
36. Zhao Y, Liu X, Li H, Zhai T, Zhou H (2012) Hierarchical micro/nano porous silicon Li-ion battery anodes. Chem Commun 48:5079–5081. doi:10.1039/c2cc31476b
37. Bang BM, Lee J-I, Kim H, Cho J, Park S (2012) High-performance macroporous bulk silicon anodes synthesized by template-free chemical etching. Adv Energy Mater 2:878–883. doi:10.1002/aenm.201100765
38. Kim J-H, Khanal S, Islam M, Khatri A, Choi D (2008) Electrochemical characterization of vertical arrays of tin nanowires grown on silicon substrates as anode materials for lithium rechargeable microbatteries. Electrochem Commun 10:1688–1690. doi:10.1016/j.elecom.2008.08.040
39. Ortiz F, Hanzu I, Knauth P, Lavela P, Tirado JL, Djenizian T (2009) TiO_2 nanotubes manufactured by anodization of Ti thin films for on-chip Li-ion 2D microbatteries. Electrochim Acta 54:4262–4268. doi:10.1016/j.electacta.2009.02.085
40. Aurbach D, Markovsky B, Salitra G, Markevich E, Talyossef Y, Koltypin M, Nazar L, Ellis B, Kovacheva D (2007) Review on electrode–electrolyte solution interactions, related to cathode materials for Li-ion batteries. J Power Sources 165:491–499. doi:10.1016/j.jpowsour.2006.10.025
41. Moshkovich M, Cojocaru M, Gottlieb H, Aurbach D (2001) The study of the anodic stability of alkyl carbonate solutions by in situ FTIR spectroscopy, EQCM, NMR and MS. J Electroanal Chem 497:84–96. doi:10.1016/S0022-0728(00)00457-5
42. Aurbach D, Moshkovich M, Cohen Y, Schechter A (1999) The study of surface film formation on noble-metal electrodes in alkyl carbonates/li salt solutions, using simultaneous in situ AFM, EQCM, FTIR, and EIS. Langmuir 15:2947–2960. doi:10.1021/la981275j
43. Ratnakumar B, Smart M, Surampudi S (2001) Effects of SEI on the kinetics of lithium intercalation. J Power Sources 97–98:137–139. doi:10.1016/S0378-7753(01)00682-6
44. Kawamura T, Kimura A, Egashira M, Okada S, Yamaki J (2002) Thermal stability of alkyl carbonate mixed-solvent electrolytes for lithium ion cells. J Power Sources 104:260–264. doi:10.1016/S0378-7753(01)00960-0
45. Lewandowski A, Swiderska-Mocek A (2009) Ionic liquids as electrolytes for Li-ion batteries—an overview of electrochemical studies. J Power Sources 194:601–609. doi:10.1016/j.jpowsour.2009.06.089
46. Sato T, Maruo T, Marukane S, Takagi K (2004) Ionic liquids containing carbonate solvent as electrolytes for lithium ion cells. J Power Sources 138:253–261. doi:10.1016/j.jpowsour.2004.06.027
47. Holzapfel M, Jost C, Prodi-Schwab A, Krumeich F, Wursig A, Buqa H, Novak P (2005) Stabilisation of lithiated graphite in an electrolyte based on ionic liquids: an electrochemical and

scanning electron microscopy study. Carbon 43:1488–1498. doi:10.1016/j.carbon.2005.01.030
48. Chakrapani V, Rusli F, Filler M, Kohl P (2012) Silicon nanowire anode: improved battery life with capacity-limited cycling. J Power Sources 205:433–438. doi:10.1016/j.jpowsour.2012.01.061
49. Borgel V, Markevich E, Aurbach D, Semrau G, Schmidt M (2009) On the application of ionic liquids for rechargeable Li batteries: high voltage systems. J Power Sources 189:331–336. doi:10.1016/j.jpowsour.2008.08.099
50. Garcia B, Lavallee S, Perron G, Michot C, Armand M (2004) Room temperature molten salts as lithium battery electrolyte. Electrochim Acta 49:4583–4588. doi:10.1016/j.electacta.2004.04.041
51. Placke T, Bieker P, Lux S, Fromm O, Meyer H, Passerini S, Winter M (2012) Dual-ion cells based on anion intercalation into graphite from ionic liquid-based electrolytes. Z Phys Chem 226:391–407. doi:10.1524/zpch.2012.0222
52. Baranchugov V, Markevich E, Salitra G, Aurbach D, Semrau G, Schmidt M (2008) In situ Raman spectroscopy study of different kinds of graphite electrodes in ionic liquid electrolytes. J Electrochem Soc 155:A217–A227. doi:10.1149/1.2828858
53. Ivanov S, Cheng L, Wulfmeier H, Albrecht D, Fritze H, Bund A (2013) Electrochemical behavior of anodically obtained titania nanotubes in organic carbonate and ionic liquid based Li ion containing electrolytes. Electrochim Acta 104:228–235. doi:10.1016/j.electacta.2013.04.115
54. Thakur M, Isaacson M, Sinsabauth SL, Wong MS, Biswal SL (2012) Gold-coated porous silicon films as anodes for lithium ion batteries. J Power Sources 205:426–432. doi:10.1016/j.powsour.2012.01.058
55. Lehmann V, Stengl R, Luigart A (2000) On the morphology and the electrochemical formation mechanism of mesoporous Si. Mater Sci Eng B69–70(11–22):18
56. Xu K, Zhang S, Jow TR (2003) Formation of the graphite/electrolyte interface by lithium bis(oxalato)borate. Electrochem Solid St 6:A117–A120. doi:10.1149/1.1568173
57. Aurbach D, Taylosef Y, Markvovsky B, Markevich E, Zinigrad E, Asraf L, Gnanaraj J, Kim H-J (2004) Design of electrolyte solutions for Li and Li-ion batteries: a review. Electrochim Acta 30:247–254. doi:10.1016/j.electacta.2004.01.090